Elevated glucocorticoid alters the developmental dynamics of hypothalamic neurogenesis

Helen Eachus[1], Min-Kyeung. Choi[1], Anna Tochwin[1], Johanna Kaspareit[2], May Ho[3], Soojin Ryu*[1,2]

* Corresponding author

[1] Living Systems Institute, University of Exeter, Stocker Road, Exeter, EX4 4QD. United Kingdom.

[2] University Medical Center, Johannes Gutenberg University Mainz, Duesbergweg 6, 55128 Mainz, Germany.

[3] Nanyang Technological University, 50 Nanyang Avenue, Singapore 639798.

Corresponding author email address: s.ryu@exeter.ac.uk

Abstract

Exposure to excess glucocorticoid (GC) during early development is implicated in adult dysfunctions. Reduced adult hippocampal neurogenesis is a well-known consequence of exposure to early life stress or elevated GC, however the effects on neurogenesis during development and effects on other brain regions are not well understood. Using an optogenetic zebrafish model, here we analysed the effects of GC exposure on neurogenesis during development in the whole brain. We identify that the hypothalamus is a highly GC-sensitive region where elevated GC causes precocious development. This is followed by failed maturation and early decline accompanied by impaired feeding, growth, and longevity. In GC-exposed animals, the developmental trajectory of hypothalamic progenitor cells is strikingly altered, potentially mediated by direct regulation of transcription factors such as *rx3* by GC. Our data provide cellular and molecular level insight into GC-induced alteration of the hypothalamic development trajectory, a process crucial for health across the life-course.

Introduction

Glucocorticoids (GC) are the key effectors of the stress response and have pleiotropic effects on the body, acting to restore homeostasis and thus allow an animal to respond adaptively to threat[1]. Since

29 the developing brain is plastic, GC exposure during early life has the potential to alter the
30 developmental trajectory of the brain. Indeed, alteration of the development trajectory may be an
31 adaptive mechanism employed by animals exposed to stress during early life. For example, antenatal
32 GC treatment has well documented effects on lung maturation, as well as other organs, in preterm
33 babies[2]. However, such treatment has also been associated with negative outcomes in later life, such
34 as increased incidence of mental health issues during childhood[3], impacted development of fronto-
35 parietal brain functions during adolescence [4], and cortical thinning in children with associated affective
36 disorders[5]. Early life GC exposure leading to adverse consequences in later life is an example of the
37 concept known as early life programming of adult disease[6,7,8,9].
38
39 One of the well-documented effects of GC exposure during early life or early life stress (ELS) is
40 reduced adult neurogenesis in the hippocampus, including reduced cell proliferation[10,11,12,13,14]. Indeed
41 adrenalectomy is sufficient to prevent reduced proliferation in chronically stressed mice, suggesting
42 that GC is the main driving force behind this phenotype[15]. In contrast, only a few studies have looked
43 at the effects of ELS or GC exposure on neurogenesis during development, but there are some
44 indications that its effects might be developmentally dynamic. Specifically, it is possible that GC-
45 induced reduction of cell proliferation is a delayed consequence of a GC-induced change to the
46 development trajectory that began in early life. Indeed, rats exposed to ELS exhibited enhanced
47 hippocampal cell proliferation and improved stress-associated behavioural performance as young
48 adults, whilst these effects were reversed by middle age[10]. A potential mechanistic explanation for the
49 ELS-induced reduction in adult hippocampal neurogenesis is that enhanced cell proliferation at an
50 earlier time-point depletes the stem cell pool over time[16].
51
52 Despite the well-documented effects of GC exposure on hippocampal neurogenesis, the effects of
53 GC exposure on other brain regions are unclear. Recently, a first study of the effects of ELS on
54 hypothalamic neurogenesis revealed that cell proliferation and numbers of hypothalamic stem cells
55 known as tanycytes were reduced in the adult mouse[17]. Tanycytes are unique radial glial-like cells
56 that line the walls of the 3rd ventricle, have NSPC (neural stem/progenitor cell) properties that persist

into adulthood, send projections into neighbouring hypothalamic nuclei and are able to sense glucose levels in the CSF[18]. Whilst most previous studies have focused on effects of stress and GC exposure on neurogenesis in the hippocampus, the aforementioned study supports that the hippocampus is not uniquely affected by stress/GC. However, whether and how GC affects hypothalamic neurogenesis during development is completely unknown.

Here we used an optogenetic zebrafish model in which endogenous cortisol level is elevated to test the hypothesis that GC exposure alters the developmental trajectory of the brain. The model utilises optogenetic manipulation of steroidogenic interrenal cells to increase the endogenous GC level during larval and juvenile stages[19]. Whilst the mammalian adrenal gland, counterpart of the fish interrenal, is known to produce GCs, mineralocorticoids (MCs), and androgens[20]; MCs and androgens are not produced by the larval zebrafish interrenal gland[21,22,23,24]. Therefore, the phenotypes observed in our model are primarily caused by GC and its downstream effectors, rather than MC or androgen over-exposure.

We found that GC exposure affected cell proliferation in a region-specific manner and that these effects were dynamic across the life-course. We found that the hypothalamus is a highly GC-sensitive brain region. In early life, we observed precocious development of the hypothalamus and hypothalamus-associated feeding behaviour in GC-exposed animals. This was followed by a rapid decline, indicated by failed hypothalamic maturation, including reduced numbers of *agrp*- and *hcrt*-expressing neurons known to regulate feeding[25,26,27], and suppressed feeding and growth. Our data uncover a tissue-specific time-dependent plasticity of the hypothalamus in response to GC and provide cellular and molecular insights for GC-induced alteration of the hypothalamic development trajectory.

Results

Neurogenesis is altered in an optogenetic zebrafish model of elevated GC

85 Our lab previously generated an optogenetic zebrafish model, *Tg(star:bPAC-2A-tdTomato)*^{uex300}, in
86 which the endogenous cortisol level can be increased specifically in response to blue light exposure
87 using an optogenetic protein *beggiatoa* Photoactivated Adenylate Cylase (bPAC) (Fig.1a)[19,28,29]. In
88 order to determine the effects of elevated GC on the brain across development, we raised transgenic
89 fish under standard aquarium lighting conditions, where the blue light component of the white light is
90 sufficient to activate bPAC, which led to significantly elevated cortisol levels in *Tg(star:bPAC-2A-*
91 *tdTomato)*^{uex300} compared with wild types from hatching through until late juvenile/early adult stage
92 (Fig.1b)[19]. *Tg(star:bPAC-2A-tdTomato)*^{uex300} raised under standard light conditions will be referred to
93 throughout as star:bPAC+ or bPAC+.
94
95 To investigate the effects of elevated GC on brain development we performed bulk RNA-sequencing
96 (RNA-seq) of whole brain samples from star:bPAC+ and wild-type fish at different developmental
97 stages[19]. Gene Ontology (GO) analysis of differentially expressed genes (DEGs) that were down-
98 regulated in star:bPAC+ brains compared with wild types were enriched for a number of biological
99 processes, including Neurogenesis at all developmental stages (GO:0022008, adjusted p-value
100 2.47E-20 at 6 days post fertilization (dpf), 5.45E-08 at 13 dpf, 1.11E-17 at 120 dpf). Up-regulated
101 genes were not enriched for GO term neurogenesis. To investigate the effects of GC exposure on
102 neurogenesis during development, we focused downstream analysis on the early life time-points: 5/6
103 dpf and 13 dpf. 225 genes associated with neurogenesis were down-regulated in star:bPAC+ brains
104 at either 6 dpf or 13 dpf (Fig.1c). To confirm our results and identify specific features of neurogenesis
105 that are altered by elevated GC, we performed qPCR on independent samples of whole brains from
106 5 dpf star:bPAC+ and wild types for genes associated with neurogenesis processes or distinct cell
107 types. Of the 14 categories of genes analysed, only one category was associated with consistent
108 differential expression in star:bPAC+. Expression of *pcna*, *mki67* and *mcm5*, all associated with cell
109 proliferation, showed increased expression in star:bPAC+ compared with wild types (Supplementary
110 Fig.1). These data support that neurogenesis, and especially cell proliferation, is altered by elevated
111 GC.
112

113 To identify whether the effect of GC on neurogenesis is developmentally dynamic, we performed
114 unsupervised clustering analysis of neurogenesis DEGs at 6 dpf and 13 dpf and identified 6 different
115 clusters. Cluster 2 and cluster 5 genes showed a relatively stronger down-regulation at 6 dpf
116 compared to 13 dpf, meanwhile cluster 1 genes showed a relatively stronger downregulation at 13
117 dpf (Fig.1d). Cluster 3 genes were strongly downregulated at both time-points (Fig.1d). Interestingly,
118 cluster 4 and cluster 6 genes showed a timepoint-specific down-regulation. Cluster 4 genes were
119 downregulated in star:bPAC+ at 6 dpf but were not differentially expressed at 13 dpf (Fig.1d).
120 Meanwhile cluster 6 genes were down-regulated in star:bPAC+ at 13 dpf but not at 6 dpf (Fig.1d).
121 These results suggest that some effects of elevated GC on neurogenesis are temporarily dynamic
122 during early life. GO analysis of genes within the clusters indicated that all clusters contained genes
123 associated with neuron differentiation (Fig.1e). Gliogenesis and glial cell development were enriched
124 in multiple clusters. There were also some terms which were restricted to single or small numbers of
125 clusters. For example, cluster 4 genes were associated with neuron fate commitment, cluster 3 with
126 neuron migration, and cluster 2 with neuronal stem cell population maintenance (Fig.1e). These
127 results suggest that specific aspects of neurogenesis exhibit temporally dynamic differential
128 expression during early life as a result of GC exposure.
129
130 **Precocious hypothalamic development following elevated GC**
131 In order to determine whether the effects of elevated GC on cell proliferation were brain-wide or region
132 specific we performed immunohistochemistry (IHC) for mitosis marker phospho-histoneH3 (pH3) on
133 brains of 5 dpf star:bPAC+ and wild-type larvae (Fig.2a). Cell counting of proliferating pH3+ cells
134 across brain regions indicated a trend towards an increase in number of pH3+ cells in the valvula
135 cerebelli (ce-v) of the hindbrain, however, the only significant increase was restricted to the
136 hypothalamus (Fig.2b). We next sought to determine which cell types were associated with the
137 increased proliferative capacity in the hypothalamus of 5 dpf star:bPAC+. To this end, we performed
138 Fluorescent *in situ* hybridization (FISH) for *rx3* (*retinal homeobox gene 3),* combined with IHC for
139 Pcna and pH3. *rx3* is a transcription factor known to be expressed in hypothalamic progenitor cells in
140 zebrafish where it plays a critical role in hypothalamic development[30], and its mammalian orthologue

141 *Rax* is known to be expressed in hypothalamic radial glia[31]. Pcna and pH3 are markers for proliferating
142 cells during S-phase and M-phase respectively. Pcna+ cells were situated around the 3rd ventricle of
143 the hypothalamus, especially around the lateral recess, in both star:bPAC+ and wild-type larvae, with
144 a small number of pH3+ cells scattered throughout this region (Fig.2c). We distinguish the Pcna+
145 region around the hypothalamic ventricles as the 'proliferative zone' and observed co-localisation of
146 *rx3* with Pcna and pH3 within the proliferative zone (Fig.2c, white arrowheads).
147
148 Quantitative analysis of confocal stacks revealed that the hypothalamus was significantly larger
149 (Fig.2f), and we found a significant increase in *rx3* and pcna signal intensity, and significantly more
150 pH3+ cells in the hypothalamus of 5 dpf star:bPAC+ compared with wild types (Fig.2g-i). To determine
151 whether the observed increase in hypothalamic proliferation in the hypothalamus of 5 dpf star:bPAC+
152 larvae is a direct effect of developmental GC exposure, we treated star:bPAC+ larvae with the GR
153 antagonist RU-486 from 2 dpf until 5 dpf. Treatment with RU-486 did not significantly affect
154 hypothalamic volume and elicited only a trend reduction in hypothalamic Pcna, however it was
155 sufficient to significantly reduce the number of pH3+ mitotic cells in the hypothalamus (Supplementary
156 Fig.2), suggesting that GR signalling is a significant driver of the increased hypothalamic proliferation
157 observed in star:bPAC+ larvae. Further, we observed that the excess hypothalamic pH3+ cells were
158 *rx3*+, meanwhile *rx3*-/pH3+ cells were not different (Fig.2i). These results suggest that excess
159 proliferating hypothalamic cells in star:bPAC+ are *rx3*-expressing radial glia. Interestingly, we
160 identified two Glucocorticoid Response Elements (GREs) within the zebrafish *rx3* gene (Fig.2l). GRE1
161 is in the 5' UTR, which is most likely a regulatory region. ChIP-qPCR analysis revealed enrichment of
162 GR antibody (compared with IgG) at both GREs in larval brain samples, supporting that GR does
163 indeed bind to regulatory regions of the *rx3* gene (Fig.2m). Further, enrichment of GR was higher in
164 dexamethasone-treated wild-type samples, compared with wild-type controls, and higher still in
165 star:bPAC+ samples. This experiment shows that GC exposure directly regulates GR-mediated
166 control of *rx3* gene expression in the brain.
167

168 Whilst *rx3* appeared to be co-expressed with Pcna in proliferating radial glia, we also analysed Blbp
169 (brain lipid binding protein, fabp7a) localisation, which is known to be expressed in predominantly
170 quiescent radial glia in the zebrafish brain[32]. Consistent with this, we observed strong expression of
171 Blbp in cells lining the third ventricle in the Pcna-negative rostral domains of the hypothalamus, whilst
172 some Blbp signal was also observed in Pcna-positive cells of the lateral recess (Fig.2d). In 5 dpf
173 star:bPAC+ larvae, we observed increased Blbp signal, especially in the arcuate region of the
174 hypothalamus (Fig.2d,j), suggesting that increased numbers of glial cells might include both
175 proliferative and quiescent subtypes. Finally we observed increased signal for Otpa (orthopedia
176 homeobox a) in the hypothalamus of 5 dpf star:bPAC+ larvae (Fig.2e,k), which is predominantly
177 expressed in early post-mitotic neuronal precursors[33], suggesting that the excess GC-exposed
178 hypothalamic proliferative radial glia do exit the cell cycle, leading to increased numbers of neuronal
179 precursors. Together these data suggest that elevated GC drives precocious development of the
180 hypothalamus in zebrafish larvae.
181
182 **Failed hypothalamic maturation following elevated GC**
183 To test whether the effects of GC exposure on hypothalamic neurogenesis might be temporally
184 dynamic, we investigated hypothalamic cell proliferation at 13 dpf. In the 13 dpf hypothalamus, *rx3*
185 was expressed in a subset of Pcna+ cells around the lateral recess, and Blbp was expressed mainly
186 along the midline 3rd ventricle anterior to the proliferative zone, in a similar manner to at 5 dpf (Fig.3a).
187 In 13 dpf star:bPAC+ larvae, we observed that the size of the hypothalamus was no longer larger,
188 which was previously observed at 5 dpf (Fig.3b). Expression of hypothalamic *rx3* was low at this
189 developmental stage, and showed a trend towards a reduction in star:bPAC+ compared with wild type
190 (Fig.3a,c). In stark contrast to the 5 dpf hypothalamus, we now observed a dramatic reduction in
191 expression of Pcna in 13 dpf star:bPAC+ hypothalamus (Fig.3a,d). Meanwhile, Blbp signal intensity
192 was not different between 13 dpf wild-type and star:bPAC+ larvae (Fig.3a,e).
193
194 Strikingly, when we performed co-expression analysis, we observed that whilst only a small proportion
195 of Blbp+ cells were proliferative in 13 dpf wild-type hypothalamus (~10%), almost all Blbp+ cells were

196 quiescent in star:bPAC+ (Fig.3f). Further, we observed that in wild types most hypothalamic *rx3*+ cells
197 (~70%) were proliferative and expressed Pcna, however in star:bPAC+ most *rx3*+ cells (~85%) were
198 quiescent and didn't express Pcna (Fig.3g). These data support that proliferative radial glia are lost
199 in the hypothalamus of 13 dpf star:bPAC+ larvae. Next, we sought to identify an explanation for the
200 loss of proliferative radial glia in the hypothalamus. We first analysed cell death in the hypothalamus
201 of 13 dpf larvae using a TUNEL assay. We did not observe a significant difference in the number of
202 apoptotic cells in the hypothalamus of 13 dpf star:bPAC+ larvae compared to wild types
203 (Supplementary Fig.3a), suggesting that loss of hypothalamic radial glia is not due to increased cell
204 death. We reasoned that the loss of proliferation in the star:bPAC+ hypothalamus might be due to
205 senescence of the formerly highly proliferative radial glia. In support of this hypothesis, we observed
206 that one of the five significantly enriched KEGG pathways in our whole brain RNA-seq data set in the
207 13 dpf star:bPAC+ was cellular senescence, a pathway which was not enriched in the 6 dpf
208 star:bPAC+ samples (Supplementary Fig.3b,c). In the RNA-seq analysis, 102 of 150 genes
209 associated with the KEGG pathway cellular senescence were differentially expressed in 13 dpf
210 star:bPAC+ brain samples, meanwhile at 6 dpf only 60 of those genes were differentially expressed,
211 and they generally showed a lesser degree of fold change (Supplementary Fig.3d). This suggested
212 that proliferative radial glia might have been lost in the hypothalamus of 13 dpf star:bPAC+ larvae due
213 to cellular senescence. Additionally, we confirmed that the loss of hypothalamic proliferation is
214 maintained into later life, since we observed that in juvenile star:bPAC+ fish, the hypothalamus is
215 smaller and contained fewer mitotic cells (Supplementary Fig.4a-c). This suggests that the
216 proliferative hypothalamic cells lost at 13 dpf do not re-enter the cell cycle later in development,
217 suggesting that they have become senescent, rather than quiescent.
218
219 Since we observed a dramatic reduction in cell proliferation in the hypothalamus of 13 dpf star:bPAC+
220 larvae, we postulated that downstream neurogenesis and neuronal differentiation might also be
221 affected. Since one of the hypothalamus-regulated functions is feeding behaviour and food intake, we
222 sought to determine whether specific neurons that regulate feeding were altered in the hypothalamus
223 of star:bPAC+ larvae at 13 dpf. *agouti-related peptide* (*agrp*) is expressed in a cluster of cells in the

224 arcuate nucleus of the hypothalamus, and we observed significantly fewer numbers of these cells in
225 star:bPAC+ larvae (Fig.3h,i). A small number of cells expressing *cart4* (*cocaine- and amphetamine-*
226 *regulated transcript*) were observed near to the medial lateral hypothalamus (mLH) and the total
227 number of these cells were also reduced in star:bPAC+ larvae (Fig.3h,j). Orexin+ (*hcrt*, *hypocretin*)
228 cells were observed in the dorso-rostral hypothalamus and we observed a trend reduction in cell count
229 in star:bPAC+ larvae (Fig.3h,k). We observed *npy* (*neuropeptide y*) cells near the mLH and these
230 cells were not affected in star:bPAC+ larvae (Supplementary Fig.5a,b). Finally, *pomca*
231 (*proopiomelanocortin*) is also expressed in the arcuate hypothalamic nucleus, and these cells were
232 not significantly reduced in star:bPAC+ larvae (Supplementary Fig.5a,c). Of the neuromodulators
233 where we observed reduced numbers in star:bPAC+, *agrp*[25,26] and *hcrt*[27] are both known to be
234 appetite-stimulators, meanwhile the effects of *cart* on appetite are more complex[34]. These data
235 indicate that neurogenesis of specific neuronal subtypes that stimulate feeding are reduced in 13 dpf
236 star:bPAC+ larvae.
237
238 **Progenitor cells fail to differentiate in the hypothalamus of star:bPAC+ larvae**
239 Since we observed that the effects of GC on hypothalamic proliferation changed dramatically between
240 5 dpf and 13 dpf, we sought to track the proliferating radial glia of the hypothalamus between these
241 timepoints to determine their fate. To do this we exposed 4 dpf larvae to BrDU (Bromodeoxyuridine)
242 overnight for 17 hours until 5 dpf and then fixed larvae at 5, 8, 10 or 13 dpf for double-IHC analysis of
243 BrDU and Pcna (Fig.4a). At 5 dpf we observed successful incorporation of BrDU into proliferating
244 cells, as observed by co-expression with Pcna, in the hypothalamus of both star:bPAC+ and wild-type
245 larvae (Fig.4b). By 8, 10 and 13 dpf, BrDU+ cells in the wild-type hypothalamus have begun exiting
246 the cell cycle and are now mostly observed around the perimeter of the Pcna-expressing proliferative
247 zone (Fig.4c, Supplementary Fig.6). Indeed, we observed that the percentage of hypothalamic BrDU+
248 cells that co-express Pcna drops from around 75% at 5 dpf to 50-55% at 8-13 dpf (Fig.4d), suggesting
249 that some of the BrDU+ cells that were proliferating at 5 dpf have lost their progenitor cell status and
250 differentiated.

251 In stark contrast, hypothalamic BrDU+ cells in star:bPAC+ larvae are still predominantly observed
252 within the Pcna+ proliferative zone after 5 dpf (Fig.4c, Supplementary Fig.6). In fact, the percentage
253 of hypothalamic BrDU+ cells that co-express Pcna remains at around 100% from 5 dpf until 13 dpf in
254 star:bPAC+ larvae (Fig.4d). This indicates that in star:bPAC+ larvae, hypothalamic progenitor cells
255 remain proliferative between 5 dpf and 13 dpf and do not differentiate. Further, we observed an
256 increase in the number of hypothalamic BrDU+ cells between 5 dpf and 8 dpf in wild types, supporting
257 that these cells are dividing and therefore increase in number, however no such increase was
258 observed in star:bPAC+ larvae (Fig.4e). Similarly, the number of hypothalamic Pcna+ cells increased
259 in wild types between 5 dpf and 10 dpf, indicating that the proliferative zone continues to expand as
260 cells divide during this period (Fig.4f). No increase in the number of hypothalamic Pcna+ cells was
261 observed in star:bPAC+ larvae during this developmental period (Fig.4f), further supporting that
262 neurogenesis appears to stall during this developmental window in star:bPAC+ larvae. Together,
263 these data support that in star:bPAC+ larvae, hypothalamic progenitor cells fail to differentiate, and
264 neurogenesis is stalled during the 5-13 dpf time window.
265
266 **Functional consequences of elevated GC: precocious feeding followed by physical decline**
267 The increased size and proliferative capacity of the hypothalamus in 5 dpf star:bPAC+ larvae
268 suggested that development of the hypothalamus is accelerated in these animals. Therefore, we
269 hypothesised that behaviours associated with the hypothalamus that develop around this
270 developmental stage might also be altered and thus we analysed feeding in 5 dpf larvae. Feeding
271 usually emerges at around 120 hpf (5 dpf) in lab-raised zebrafish larvae, and larvae are capable of
272 eating small live food. We exposed 5 dpf larvae to live rotifers and saw that star:bPAC+ larvae
273 consumed significantly more rotifers during the trial (Fig.5a), suggesting that GC-induced precocious
274 hypothalamic development is accompanied by early emergence of an associated behaviour, feeding.
275
276 In light of the reduction of cells expressing feeding-related neuromodulators in the hypothalamus of
277 13 dpf star:bPAC larvae, we sought to determine whether feeding was also affected at 13 dpf. In stark
278 contrast to 5 dpf, at 13 dpf star:bPAC+ larvae fed less than wild types (Fig.5b). Interestingly, in 13 dpf

279 wild-type larvae we observed that food intake positively correlated with body size, in that larger larvae
280 ate more, whilst in star:bPAC+ larvae no significant trend was apparent. (Fig.5c). Hence, star:bPAC+
281 larvae consumed less, regardless of their size. Whilst at 5 dpf and 13 dpf we did not observe any
282 difference in larval body size, at 28 dpf and 120 dpf star:bPAC+ fish were significantly smaller than
283 wild types (Fig.5d). This suggests that the reduction in food intake in star:bPAC+ animals from 13 dpf
284 ultimately leads to impaired growth. Finally, we also observed reduced fertilisation rates and reduced
285 long-term survival of star:bPAC+ fish (Fig.5e,f). Together, these results point towards potential
286 functional consequences of failed hypothalamic development after 5 dpf, including impaired behaviour
287 and an early physical decline. Further work is required to directly link altered hypothalamic
288 neurogenesis with the observed functional alterations in GC-exposed animals.
289

290 **Discussion**

291 This work shows for the first time that elevated glucocorticoid alters the trajectory of hypothalamic
292 development and function. We identify that the hypothalamus is a highly GC-sensitive region where
293 elevated GC causes precocious development followed by failed maturation and early decline
294 accompanied by impaired feeding, growth, and longevity.
295

296 Whilst others studies have reported GC-induced reduction in cell proliferation[35], our data supports the
297 hypothesis that, at least in some cases, the reduced cell proliferation following GC exposure might be
298 a consequence of a prior increase in proliferation. Indeed the concept of GC-inducible stem cells is
299 not novel[36,37], and there are many reports of a GC-induced increase in cell proliferation of various cell
300 types including NSPCs[38,39,40,41]. The initial GC-induced increase in cell proliferation observed here
301 might be in part mediated by mechanisms akin to those observed during brain injury, whereby formerly
302 quiescent radial glia enter the cell cycle in response to trauma[32,42]. In the published literature, there
303 are very few previous studies of effects of GC on cell proliferation across development. Of those,
304 Noorlander *et al.*, observed that antenatal GC treatment in mice led to an initial reduction in cell
305 proliferation in the embryonic hippocampus, followed by increased cell proliferation during the
306 postnatal period and a subsequent reduction in proliferation during adulthood[43]. There are also

307 examples in mouse models where ELS induced an initial increase in cell proliferation in the
308 hippocampus during early life which was again followed by a subsequent reduction in cell
309 proliferation[10] or hippocampal volume[12] in later life. Further, a meta-analysis of age-dependent effects
310 of ELS on cell proliferation shows a negative correlation between age and change in cell proliferation,
311 with the ELS-exposed animals analysed earliest in development exhibiting increased cell proliferation
312 and older ELS-exposed animals exhibiting a reduction in cell proliferation[44]. It is possible that our
313 interpretation of the results presented here also applies to other studies, in that GC drives precocious
314 proliferation leading to failed maturation and a rapid decline. In human hippocampal progenitor cells,
315 a low dose of GC was found to enhance cell proliferation, via MR function, meanwhile a higher dose
316 of GC was reported to diminish cell proliferation, via GR function[45]. Whilst these results support a
317 dichotomy of effects on proliferation resulting from low and high dose GC treatment, it is plausible that
318 a similar phenomenon might occur in response to short-term and long-term exposure to GC, as is
319 seen in our contrasting data from the 5 dpf and 13 dpf GC-exposed hypothalamus. Indeed, further
320 work *in vitro* supports that the effects of GC on neurogenesis can vary depending on the timing of GC
321 treatment[46].
322
323 In our model, we observed profound effects on a population of NSPCs within the proliferative zone of
324 the developing hypothalamus. Indeed this population of hypothalamic radial glia might be akin to
325 tanycyte cells observed in mammals, which also express *Rax*/*rx3* and *Blbp*[18], and were recently
326 shown to be sensitive to ELS exposure in adult mice[17]. We postulate that these cells might be
327 especially sensitive to the effects of elevated GC, since they are adjacent to the 3rd ventricle and thus
328 might detect elevated GC levels within the CSF. Indeed, neurogenesis of tanycyte cells is even
329 responsive to dietary cues[47]. Another potential driver of increased sensitivity of the hypothalamus to
330 GC would be increased levels of GR, however, it is not currently clear whether the hypothalamus
331 expresses higher levels of GR than other brain regions in zebrafish, or indeed in other vertebrates.
332 As such, an explanation for the specificity of the proliferation phenotype observed in our study remains
333 elusive. We cannot rule-out the possibility that the hypothalamus is not uniquely affected in our model,
334 but rather that the effects of GC on different brain regions might emerge across different time-scales.

335

336 We observed significant effects on feeding behaviour of developmental GC-exposed star:bPAC+
337 larvae, whereby 5 dpf larvae consumed more and 13 dpf larvae consumed less than controls. The
338 observed reduction in feeding persists into adulthood in this model[19]. These changes correlated with
339 increased proliferative hypothalamic radial glia at 5 dpf, which were reduced by 13 dpf, alongside a
340 reduction in numbers of feeding-regulating neurons that express *agrp*, *cart* and *hcrt at* 13 dpf. The
341 role of these hypothalamic neuropeptides in food consumption in mammals is well established[48,49,50].
342 In larval zebrafish, hypothalamic *agrp* neurons are known to stimulate feeding[25,26], and orexin,
343 produced by *hcrt* neurons, is also known to stimulate food intake in zebrafish[27]. As such, it is likely
344 that the observed reduction in numbers of *agrp* and *hcrt* neurons in 13 dpf star:bPAC+ larvae underlie
345 the observed reduction in food consumption at the same developmental stage. Another hypothesis
346 regarding the basis of the altered food consumption in the star:bPAC+ larvae relates to the observed
347 changes in hypothalamic radial glia. The population of hypothalamic radial glia altered by
348 developmental GC exposure in our model display similarities to mammalian tanycyte cells, based on
349 location, morphology, and marker expression[18]. Recent work demonstrated that hypothalamic
350 tanycytes can regulate food intake[51]. Hypothalamic tanycytes are known to project to neighbouring
351 orexigenic *npy*/*agrp* and anorexigenic *pomc* neurons of the arcuate nucleus, and tanycyte activation
352 was shown to depolarise these neurons *in vitro*, and lead to hyperphagia *in vivo*. It is interesting to
353 postulate that if similar functionality occurs in the hypothalamic radial glia of zebrafish, then the
354 observed increase in these cells at 5 dpf might contribute to the increased feeding behaviour
355 observed, meanwhile the subsequent reduction of these cells might contribute to the reduction of
356 feeding behaviour observed in 13 dpf star:bPAC+ larvae. Further work is required to characterise the
357 development and function of the zebrafish hypothalamic radial glia, and to determine the mechanisms
358 underlying the altered feeding observed in star:bPAC+ larvae.

359

360 We hypothesise that the precocious hypothalamic development observed here may represent an
361 example of GC-induced adaptive plasticity (Fig.6), as observed in other animals. For example in red
362 squirrels, females exposed to high-density cues (mimicking increased competition) increase their

363 levels of endogenous GC which drives them to produce offspring that grow faster than controls[52]. This
364 so-called adaptive plasticity is acknowledged to have short-term fitness benefits, but the investment
365 is often associated with costs in later life[53]. The costs of accelerated development can include reduced
366 longevity, which is known as the growth-rate lifespan trade-off[54], as well as reductions in breeding
367 success[55]. Interestingly, there is evidence directly linking divergence from the normal growth trajectory
368 with longevity, since sticklebacks that are forced to grow faster have a reduced lifespan, whilst those
369 in which growth was slowed down lived longer than controls[54]. In our model, chronic GC exposure
370 ultimately appears to lead to allostatic overload, a maladaptive state whereby an organism can no
371 longer adapt to its conditions[56]. Whilst GC-induced acceleration of growth-rate leading to adverse
372 phenotypes later is widely observed at the organism level, the underlying cellular and molecular
373 mechanisms are poorly understood. Our work provides new insight into these processes in the
374 developing brain.
375
376 In the context of the early-late life trade-off, the subsequent reduction in breeding success and/or
377 longevity is thought to be related to oxidative stress[57,58]. Exposure to elevated GC is known to increase
378 oxidative stress[59], a phenomenon in which an over-accumulation of reactive oxygen species (ROS)
379 occurs in cells and tissues[60]. ROS is known to cause cellular damage, especially to DNA, and can
380 lead to accelerated telomere shortening[61]. In a previous study of amphibian larvae, the relationship
381 between stress, development, growth and aging depended on the type of stressor exposure[62].
382 Predator exposure initiated faster development and enhanced growth of survivors, but they showed
383 signs of oxidative stress, had shorter telomeres and reduced long-term survival[62]. This indicates that
384 stress exposure may initiate faster development in early life, but at a cost to long-term health and
385 longevity.
386
387 Telomeres shorten with every round of cell division and when a critical size is reached this imposes
388 a functional limit on cell replication, leading to replicative senescence, which can contribute to age-
389 related diseases[61]. One possibility in our model is that the excess proliferation of hypothalamic
390 progenitors observed in 5 dpf star:bPAC+ larvae leads to subsequent senescence of those cells. In

391 contrast to quiescent, apoptotic, or terminally differentiated cells, senescent cells have incurred an
392 irreversible cell cycle arrest, yet remain viable, have alterations in metabolic activity and undergo
393 dramatic changes in gene expression[63]. In support of our hypothesis, a previous study of liver
394 progenitor cells reported that GC exposure induced cell proliferation leading to long-term replicative
395 senescence/stemness exhaustion[64], and GC is also reported to induce senescence of NSPCs *in*
396 *vitro*[65]. The presence of senescent cells in the proliferative zone of the GC-exposed hypothalamus at
397 13 dpf might explain why we observed reduced expression of Pcna and *rx3*, and a reduced
398 proliferative capacity of the remaining glial cells in the proliferative zone of star:bPAC+ larvae.
399 Telomere shortening and senescence are associated with aging and age-related diseases; and
400 models of accelerated aging present with phenotypes such as reduced longevity and physical
401 decline[66], as observed in our model. Additionally, chronic exposure to GC is associated with signs of
402 accelerated aging at a cellular level[67]. Further analysis of oxidative stress and telomere homeostasis
403 would provide further insight into the mechanisms underlying the phenotypes observed here.
404
405 We conclude that the phenotypes observed in our optogenetic model are the result of exposure to
406 elevated GC produced in the interrenal, rather than to other interrenal steroid hormones, which are
407 not detectable in larval zebrafish[19,68,69]. We propose that GC-induced alteration of the hypothalamic
408 development trajectory observed in our model is mediated by GR-regulated gene transcription and
409 potentially epigenetic mechanisms. In support of this, we showed that treatment with GR antagonist
410 RU-486 reduced the number of pH3+ mitotic cells in the hypothalamus of star:bPAC+ larvae. We also
411 provide evidence for regulation of hypothalamic *rx3* by GR. Indeed, GR signalling is known to regulate
412 cell cycle progression in NSPCs by inducing a specific pattern of DNA methylation during aging[70]. In
413 a model of replicative senescence, GC exposure lead to altered methylation of GR target gene *fkbp5*,
414 which was exacerbated by age, and the subsequently increased *fkbp5* expression was associated
415 with inflammation and myocardial infarction in humans, suggesting that GC is linked with age-related
416 disease via a mechanism involving epigenetic regulation of *fkbp5*[71]. Meanwhile in cancer cells, GC
417 exposure can induce a cell dormancy state which is in part senescence and in part quiescence,
418 mediated by GR target gene *CDNK1C* (*cyclin-dependent kinase inhibitor 1C)*[72], further supporting

419 that GC exposure might regulate cell proliferation in our model via GR-mediated regulation of cell
420 cycle.
421
422 We speculate that the effects of elevated GC on the hypothalamic development trajectory reported
423 here might be an example of allostatic overload. Allostasis is the process of activating adaptive
424 mechanisms in response to external or internal changes, however prolonged exposure to stressors
425 can lead to accumulation of so-called allostatic load, and subsequently a maladaptive state of
426 allostatic overload[8], which is associated with age-related diseases and reduced longevity. In support
427 of this, it has been proposed that effects of stress or GC on NSPCs in young individuals may affect
428 their renewal potential in the long-term, predisposing to adult disease[36]. We hypothesise that whilst
429 precocious hypothalamic development induced by GC might be an example of adaptive plasticity in
430 the short-term, the cost of this may be paid in later life through subsequent replication senescence of
431 those cells, leading to failed hypothalamic maturation, subsequent impaired feeding behaviour and
432 ultimately physical decline (Fig.6). Further understanding of how stress and GC exposure can alter
433 development trajectories at the molecular and cellular level is of critical importance to reduce the
434 burden of mental and physical ill health across the life-course.
435
436 **Methods**
437
438 **Zebrafish Husbandry and Maintenance**
439 Zebrafish experiments were performed at the University of Exeter Aquatic Resource Centre and at
440 the Johannes Gutenberg University of Mainz in compliance with local and national animal welfare
441 laws, guidelines, and policies and approved by local government (Landesuntersuchugsamt
442 Rheinland-Pfalz, Germany – 23 177-07/G20-1-033 and Home Office PPL number: PEF291C4D).
443 *Tg(2kbStAR:bPAC-2A-tdTomato)*^{uex300} were bred with wild-type TU zebrafish strain and were
444 screened at 4 dpf on a fluorescent stereomicroscope. Adult zebrafish were maintained under standard
445 zebrafish husbandry conditions, under a 12:12 light/dark cycle[73].
446

447 **RNA sequencing**

448 RNA sequencing data was obtained from our other study[19], which is deposited in the European
449 Nucleotide Archive (ENA, PRJEB53713). The detailed protocol for sample collection, RNA
450 preparation, mRNA sequencing, and bioinformatic analysis is available in an online methods
451 repository[74].

452

453 **Gene Ontology analysis**

454 The functional enrichment analysis was performed using g:Profiler (version
455 *e107_eg54_p17_bf42210)* with an adjusted p-value of 0.05. For GO analysis of neurogenesis gene
456 clusters (Fig1e), significant GO terms for each cluster were manually slimmed according to QuickGO
457 ancestor charts. Heatmaps were generated in R using the heatmap.2 function.

458

459 **qPCR**

460 Fish were immobilised using ice-cold water and larvae or dissected juvenile/adult brains were stored
461 in RNA later solution. Sample collection was carried out between 08:00 and 10:00. Larvae were
462 subsequently dissected, such that each replicate consisted of 15 larval heads (eyes and jaw removed)
463 or 3 juvenile/adult brains. RNA was extracted using TRIzol™ Reagent (Invitrogen™, 15596026), as
464 previously described[75], and cDNA was synthesised using High-Capacity RNA-to-cDNA™ Kit (Applied
465 Biosystems, 4387406). Approximately 100 ng cDNA was used in a 10 μl qPCR reaction with
466 PowerUp™ SYBR™ Green Master Mix (A25778, Applied Biosystems). Primer sequences can be
467 found in Supplementary table 1. The reactions were run in Hard-Shell 96-Well PCR Plates (HSP9601,
468 BioRad) on a CFX96 Real Time PCR machine (Bio-Rad) using a standard protocol. Relative
469 expression was calculated using the $2^{-\Delta\Delta Ct}$ method, with *18s* as a reference gene.

470

471 **Fluorescent in situ hybridisation (FISH) and immunohistochemistry (IHC)**

472 The FISH and IHC methods were based on a protocol by Jakob von Trotha (2016) for whole zebrafish
473 embryos and larvae. Larvae or juvenile fish were immobilised in ice-cold water and then whole larvae

474 or dissected juvenile fish brains were fixed in 4% PFA overnight at 4 °C, dehydrated in methanol and
475 subsequently stored at -20C. After rehydration, larvae or brains were permeabilised using proteinase
476 K (10 μg/ml) treatment at 37 °C and then re-fixed in PFA. DIG-conjugated mRNA probes were
477 hybridised overnight at 65 °C. *In situ* hybridisation probes for *rx3*, *agrp*, *cart4, npy* were synthesised
478 using primers listed in Supplementary Table 1. *pomc* probe was synthesised from a plasmid, as
479 previously described[76]. After removal of probe and washing, samples were blocked for 2 hours in
480 blocking solution (1% blocking reagent; (Roche, 11096176001) in malic acid buffer (0.15M maleic
481 acid, 0.15M NaCl, PH 7.5)) and then incubated overnight at 4 °C in anti-DIG POD antibody (Roche,
482 11207733910) diluted 1:300 in blocking solution. After more washing, samples were incubated for 40
483 minutes in the dark with 1:200 FITC-tyramide (synthesised from product 46410, Thermo Scientific),
484 0.003% H2O2, 2% dextran sulphate in PBST. For IHC antigen retrieval was performed according to
485 published methods[77]. Samples were blocked in 10% Normal goat serum in PBST for 2 hours before
486 incubation in primary antibody overnight at 4 °C. For IHC of BrDU-treated samples, samples were
487 treated with 1N HCl for 30 minutes prior to blocking. Primary antibodies used were: pH3
488 (Merck/Millipore, 06-570), pcna (Sigma, MABE288), BLBP (Sigma, ABN14), otpa[78], BrDU (abcam,
489 ab6326). After washing all day, samples were incubated overnight in 1:1000 secondary antibody with
490 1:200 hoechst (H3570, Invitrogen). Secondary antibodies used were Goat anti-Rabbit IgG (H+L)
491 Cross-Adsorbed Secondary Antibody, Alexa Fluor™ 488 (A-11008, Invitrogen), Goat anti-Rabbit IgG
492 (H+L) Cross-Adsorbed Secondary Antibody, Alexa Fluor 633 (A-21070, Invitrogen), Goat anti-Mouse
493 IgG (H+L) Cross-Adsorbed Secondary Antibody, Alexa Fluor 568 (A-11004, Invitrogen), Goat anti-
494 Rat IgG (H+L) Cross-Adsorbed Secondary Antibody, Alexa Fluor 488 (A-11006, Invitrogen). After
495 staining all samples were washed further then cleared overnight in glycerol. Samples were imaged
496 on a Zeiss LSM 880 confocal microscope using a 25x or 10x objective.
497
498 **Image processing**
499 Image processing was performed in Fiji (ImageJ2, version 2.9.0). For whole brain counting of cells,
500 z-stacks were taken across the brain from dorsal to ventral and regions were defined using the

501 hoechst staining with the Z-Brain viewer[79]. Images were thresholded and PH3 cells in each region
502 were manually counted in a blinded manner. For counting of cells within the hypothalamus, cell counts
503 were performed manually from z-stacks, in a blinded manner. Similarly, hypothalamic volume was
504 calculated based on hoechst staining in z-stacks, using Z-Brain viewer. Corrected Total Cell
505 Fluorescence (CTCF) was calculated as Integrated Density of cells – (Area of cells X Mean
506 fluorescence of background reading). For CTCF calculations, labelled cells were identified first by
507 thresholding each image and creating ROIs of the labelled cells using the Analyze Particles function.
508 The total Integrated density and total area of all labelled cells was then used to calculate CTCF for
509 each sample. For co-expression analysis, ROIs of labelled cells were generated for each marker as
510 described above. Percentage overlap was calculated using the Analyze Particles function with ROIs
511 of marker 1 cells against a mask of marker 2 cells. Total area of cells was calculated from the
512 thresholded mask/ROIs of labelled cells. pH3 cells were manually scored as *rx3*- or *rx3*+ using the
513 ROIs/masks as described above, in a blinded manner. All measures are normalised relative to size
514 of the hypothalamus.
515
516 **Feeding behaviour**
517 Prior to behavioural analysis, larvae were transferred to 24 well cell culture plates (83.3922, Sarstedt)
518 with 1 larva per well in 1.5 ml aquarium water. Larvae were then left to acclimate to the behavioural
519 testing room (maintained at 28 °C) for 2 hours. 5 dpf larvae were fed 1 ml of diluted live rotifers
520 (approximately 20), meanwhile 13 dpf larvae were fed 5 live artemia. Larvae were recorded for 10
521 minutes using Basler Video Recording Software. The camera used was a Basler (Germany) acA1300-
522 200um USB 3.0 camera with ON Semiconductor PYTHON 1300 CMOS sensor (203 frames per
523 second at 1.3 MP resolution) with a Computar Zoom Lens 18-108/2.5 (Japan). Number of successful
524 and unsuccessful prey captures and latency to first hunting attempt were analysed manually from
525 video recordings in a blinded manner.
526
527 **BrDU experiment**

528 Larvae were transferred to a 12 well dish with 10 larvae per well. Larvae were incubated overnight
529 from 4 dpf in 3 ml 10 mM 5-Bromo-2′-deoxyuridine (B5002, Sigma) with 1% DMSO for 17 hours. On
530 the morning of 5 dpf, BrDU was removed by washing 3-times with aquarium water. Larvae were
531 subsequently fixed in PFA or raised until a later stage for fixation.
532
533 **Drug treatments**
534 Larvae were incubated from 6 hpf until 120 hpf with 50 μM dexamethasone (Sigma-Aldrich D2915)
535 or from 48 hpf until 120 hpf with 2 μM RU-486 (Sigma-Aldrich, M8046). DMSO solution was used as
536 a control. Solutions were changed daily.
537
538 **ChIP-qPCR**
539 We analysed the sequence for the *rx3* gene (ENSDARG00000052893,
540 chromosome:GRCz11:21:10755554:10759823:1). Primers for *rx3* GRE1 and GRE2 are described in
541 supplementary table 1 and were designed using Primer3. GR bounded chromatin was prepared
542 following the protocol from Idilli *et al*., 2020[80], with minor modifications. For each sample, 100
543 dissected 5 dpf larval heads (without eyes) were incubated for 10 minutes at room temperature in 1%
544 formaldehyde in PBS with protease inhibitors (A32955, Thermo Scientific) for cross-linking. We used
545 a glucocorticoid receptor polyclonal antibody (24050-1-AP, Proteintech) and Rabbit IgG Isotype
546 Control (10500C, Invitrogen) as primary antibodies.
547
548 **TUNEL assay**
549 Apoptotic cells were labelled using the In Situ Cell Death Detection Kit, Fluorescein (11684795910,
550 Roche). Larvae were first fixed, dehydrated, rehydrated and permeabilised as per the FISH protocol.
551 Larvae were incubated in TUNEL reaction mix at 37 °C for 2 hours and subsequently, washed and
552 cleared as per the FISH protocol.
553
554 **Statistics**

All analyses and graphs were generated in R (RStudio 2022.07.2). Prior to testing for statistically significant differences between groups, data were tested for normality and variance. Where data did not fit the assumptions for t-testing or ANOVA, non-parametric alternatives were used. Where appropriate, Bonferroni correction for multiple testing was used. In all bar graphs mean +/- standard error is presented for each group.

561 **Figures & Figure Legends**

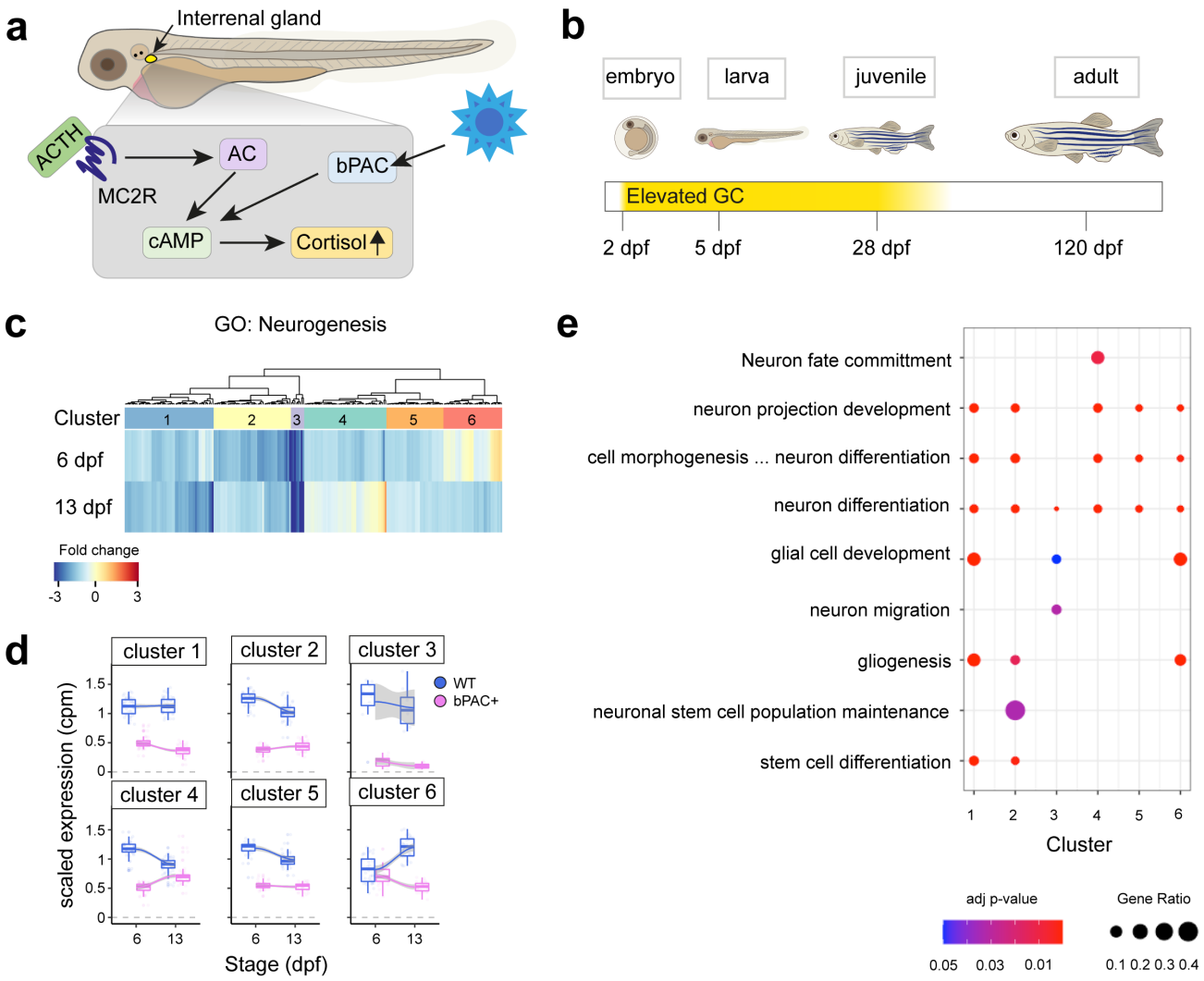

562

563 **Figure 1. Neurogenesis is altered in an optogenetic zebrafish model of elevated GC.**

564 **a**. In star:bPAC+ larvae, blue light activates cAMP signalling in the interrenal gland, which leads to
565 release of cortisol. Figure adapted from Eachus et al, 2021[81]. **b.** Wild-type and star:bPAC+ larvae
566 were raised under a standard 12:12 light/dark cycle under white light. In these conditions, basal
567 cortisol levels are elevated in star:bPAC+ larvae from 2 dpf until approximately 2 months of age. **c.**
568 Heatmap showing fold change for 225 genes associated with GO:0022008 (neurogenesis) in
569 star:bPAC+ whole-brain samples that were downregulated at either 6 dpf or 13 dpf (or both), relative
570 to wild type, from an RNA-sequencing analysis. **d.** Scaled expression (cpm) of neurogenesis-
571 associated genes in star:bPAC+ and wild-type whole-brain samples at 6 dpf and 13 dpf, according to
572 the 6 clusters shown in c. Boxes show the median and quartiles, whiskers are inter-quartile range and

573 gray shading shows the smoothed conditional means. **e**. Significant slimmed neurogenesis child GO
574 terms at $p<0.05$, identified using g:Profiler, are shown for each cluster. Size of the dot indicates the
575 ratio of differentially expressed genes from each GO term, whilst the colour shows the adjusted p-
576 value.
577

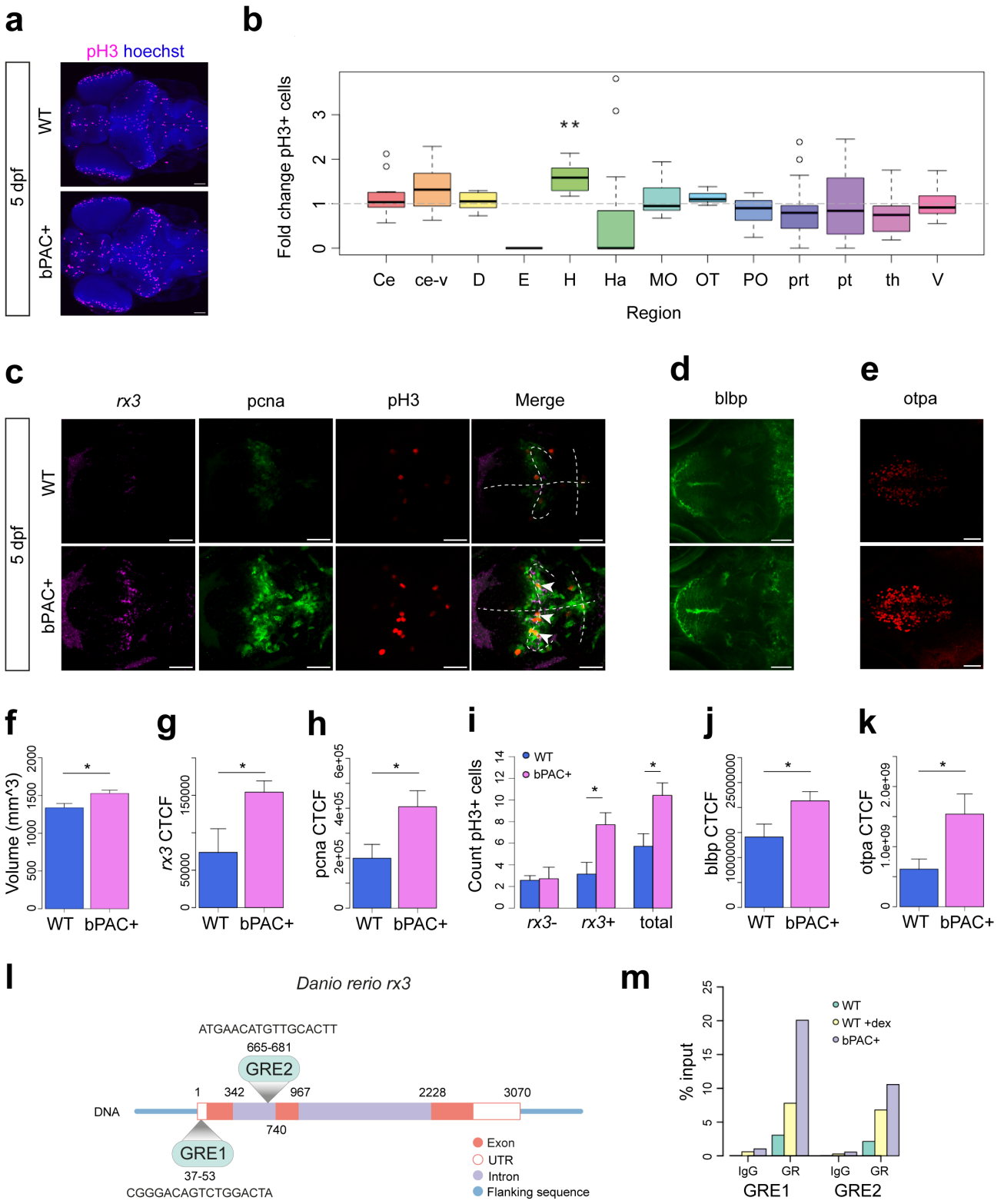

Figure 2. Precocious hypothalamic development following elevated GC.

a. Whole-brain IHC for proliferation marker pH3 as seen in a maximum intensity projection in 5 dpf wild-type and star:bPAC+ larvae. Scale bar is 60 μm. **b.** Cell counting of pH3 across brain regions revealed an increase in the hypothalamus (H) of 5 dpf star:bPAC+ larvae, compared with wild type

583 (Wilcox Exact test with Bonferroni correction (N=14, p= 0.0013195). Brain regions are labelled
584 according to the ZFIN anatomy database. **c**. Co-expression of *rx3*, pcna and pH3 in the hypothalamus
585 of 5 dpf wild-type and star:bPAC+ larvae, observed in a single plane image of FISH-IHC. Scale bar
586 40 μm. Dashed line indicates the ventricles and arrowheads indicate excess *rx3*+ pH3+ cells in
587 star:bPAC+ hypothalamus. **d.** IHC for blbp in the arcuate nucleus of 5 dpf wild-type and star:bPAC+
588 larvae, observed in a single plane image. Scale bar 40 μm**. e.** IHC for otpa in the hypothalamus of 5
589 dpf wild-type and star:bPAC+ larvae, as observed in a maximum intensity projection. Scale bar 40
590 μm**. f-h**. The hypothalamus of 5 dpf star:bPAC+ larvae is larger (f, t= -2.6193, df= 11.207, p-value =
591 0.02353) and has increased intensity of *rx3* (g, N=7, t= -2.3011, df= 8.5909, p-value = 0.04823) and
592 pcna (h, N=7, t =-2.4409, df= 11.766, p-value = 0.03147). **i.** Excess proliferating pH3+ cells in the
593 hypothalamus of 5 dpf star:bPAC+ larvae are *rx3*+ radial glia (N=7, Two-way ANOVA with Tukey's
594 test: total pH3+ cells (p= 0.0293550), *rx3*+ pH3+ cells (p= 0.0373125)). **j-k.** Intensity of blbp (j, N=9,
595 t= -2.2734, df= 14.903, p-value= 0.03823) and otpa (k, N=12, t= -2.44, df= 16.227, p-value= 0.02652)
596 was increased in the hypothalamus of 5 dpf star:bPAC+ larvae. **l.** The zebrafish *rx3* gene contains
597 two GREs, one in exon one and another in intron one. The region shown is ENSDARG00000052893,
598 GRCz11:21:10755554:10759823:1 (including flanking sequence). **m.** ChIP qPCR analysis of two
599 GREs in the *rx3* gene shows enrichment for GR compared with IgG control in 5 dpf wild-type brains.
600 Enrichment of GR was higher in wild types exposed to dexamethasone, and higher still in star:bPAC+
601 brains for both GREs.
602

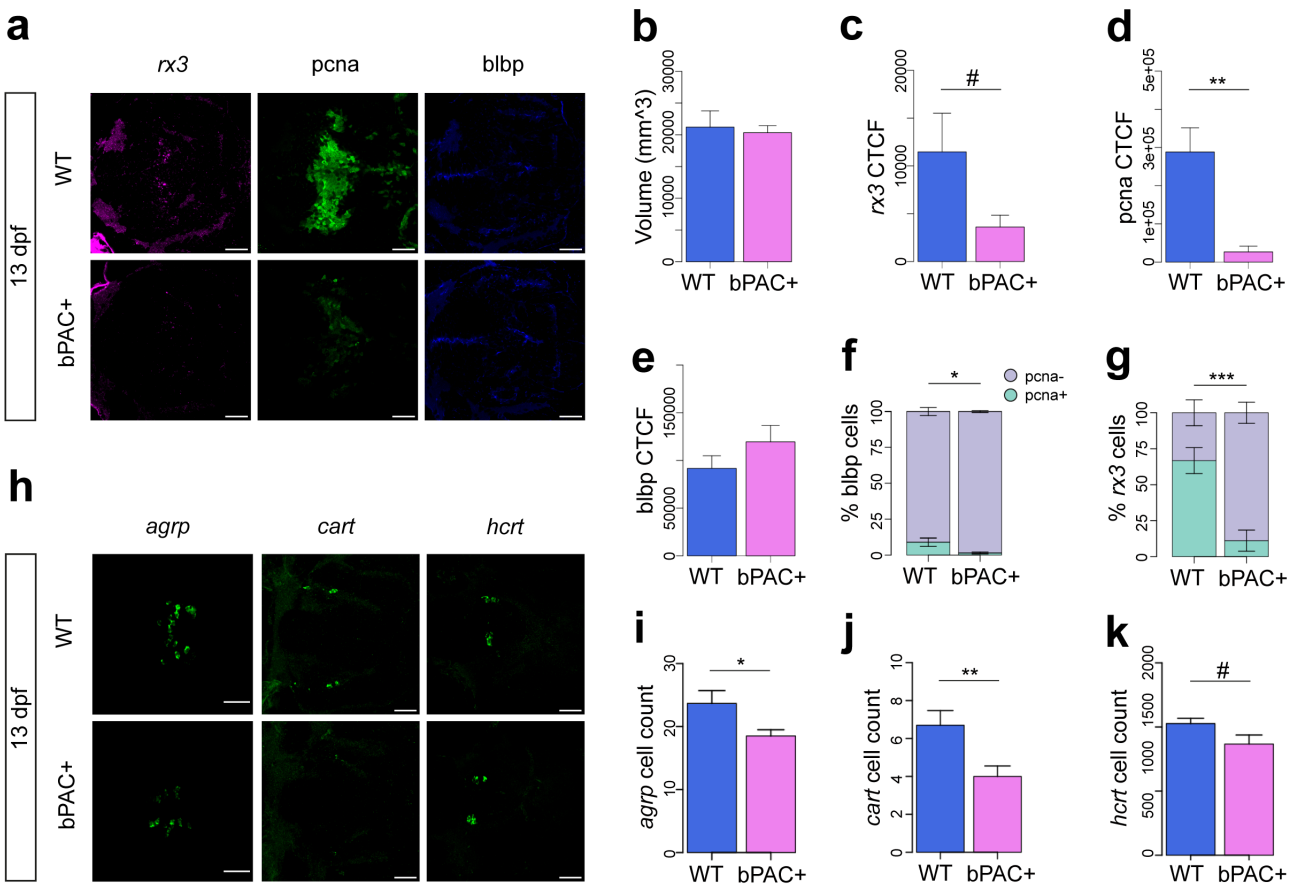

Figure 3. Failed hypothalamic maturation following elevated GC.

a. Expression of *rx3*, pcna and blbp in the hypothalamus of 13 dpf WT and star:bPAC larvae, observed via FISH-IHC in single plane confocal images through the hypothalamus. Scale bar is 40 μm. **b-e.** Quantitative analysis of confocal images shown in (a), N=8. Volume of the hypothalamus is not different (b, t = 0.31771, df = 10.899, p-value = 0.7567), meanwhile, *rx3* CTCF shows a trend towards reduction (c, t = 1.8613, df = 8.3108, p-value = 0.09835), pcna CTCF is significantly reduced (d, t = 4.0207, df = 7.7651, p-value = 0.00408), and blbp CTCF is not significantly different (e, t = -1.2827, df = 13.092, p-value = 0.2219) in the hypothalamus of 13 dpf star:bPAC+ larvae compared with wild types. **f-g.** Quantitative analysis of co-expression of pcna in hypothalamic radial glia, from the images shown in (a). blbp cells (f, t = -2.5888, df = 7.5126, p-value = 0.0339) and *rx3* cells (g, t = 4.7867, df = 13.444, p-value = 0.0003238) have a significant reduction in pcna co-expression in the hypothalamus of 13 dpf star:bPAC+ larvae compared with wild types. **h.** Expression of genes involved in feeding regulation in the hypothalamus of 13 dpf star:bPAC+ and wild-type larvae as shown in maximum intensity projections of confocal stacks. Scale bar is 40 μm. **i-k.** Quantitative analysis of

618 cell counts in the stacks shown in (h). Number of *agrp* cells is significantly lower (i, N=6-9, t = 2.2891,
619 df = 11.255, p-value = 0.04234), number of *cart4* cells is significantly reduced (j, N=20-21, t = 2.8544,
620 df = 34.862, p-value = 0.007212), number of *hcrt* cells shows a trend reduction (k, N=15-18, t = 1.9553,
621 df = 26.571, p-value = 0.06115). All graphs show the mean with standard error. #, p<0.1, *, p<0.05,
622 **, p<0.01, ***, p<0.001.
623
624

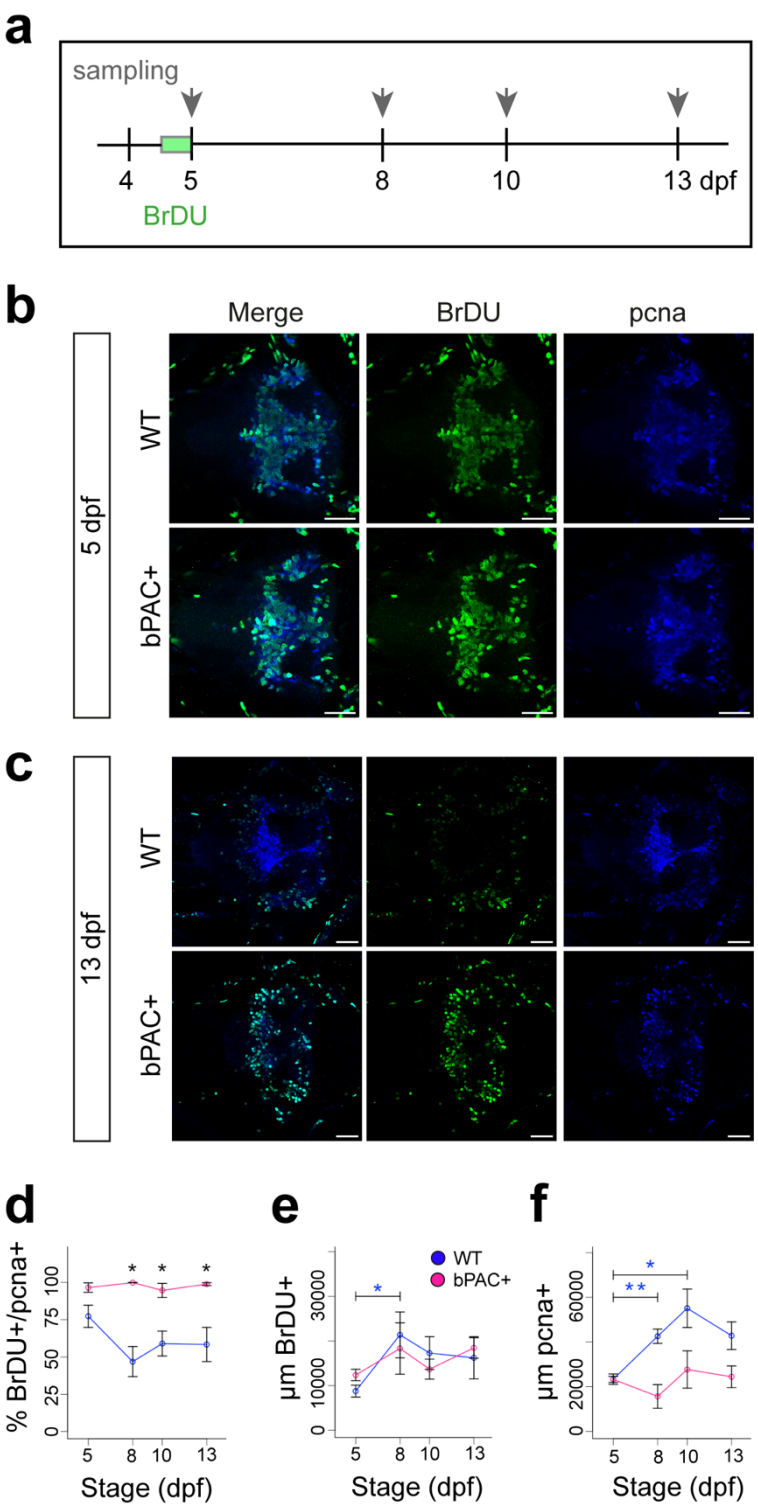

625

626 **Figure 4. Progenitor cells fail to differentiate in the hypothalamus following elevated GC.**

627 **a**. Schematic showing the experimental paradigm. Wild-type and star:bPAC+ larvae were treated with

628 BrDU overnight from 4 dpf until 5 dpf for 17 hours. Following removal of BrDU compound, larvae were

629 collected at 5 dpf, 8 dpf, 10 dpf and 13 dpf for lineage tracing analysis. **b,c.** Confocal images of BrDU

630 lineage tracing analysis at 5 dpf (b) and 13 dpf (c). In each panel wild types are shown in the upper
631 row and star:bPAC+ larvae in the bottom row. The left-most column (Merge) shows the overlap
632 between BrDU-labelled cells with endogenous pcna, whilst single channel images for BrDU and pcna
633 are adjacent. All images are a single plane from a confocal z-stack. In all cases the scale bar indicates
634 40 μm. **d-f.** Quantitative analysis of BrDU cell fate. Whilst the percentage of BrDU cells expressing
635 pcna decreases over time in wild types, this remains high in star:bPAC+ (d). Whilst BrDU+ cells
636 increase between 5 dpf and 8 dpf in wild types, this does not occur in star:bPAC+ (e). Similarly, pcna+
637 cells increase between 5 dpf and 10 dpf in wild types, but not in star:bPAC+ larvae (f). Wild types are
638 shown in blue, star:bPAC+ in pink. All graphs show the mean with standard error. N=5-10 per group.
639 *, $p<0.05$, **, $p<0.01$ for t-tests with Bonferroni correction.
640
641

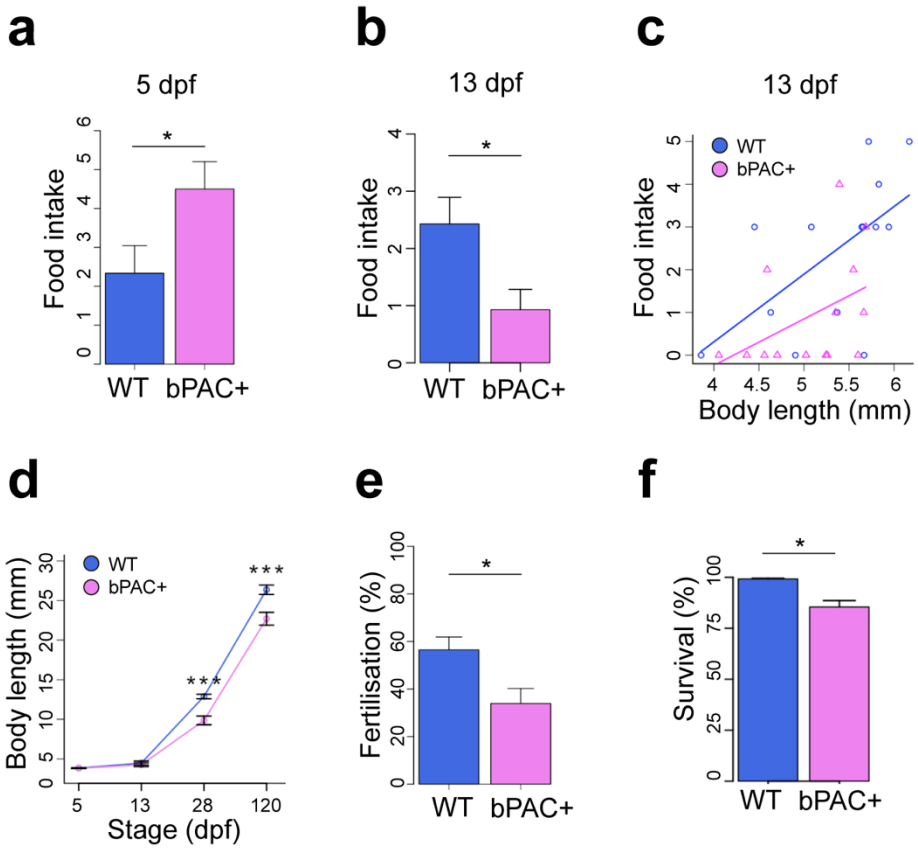

Figure 5. Functional consequences of elevated GC: precocious feeding followed by physical decline.

a. Analysis of feeding behaviour reveals that 5 dpf star:bPAC+ larvae eat more (N=12, t = -2.1694, df = 21.996, p-value = 0.04113). **b.** Analysis of feeding behaviour in 13 dpf wild-type and star:bPAC+ larvae reveals that food intake is significantly reduced (N=14, t = 2.5626, df = 24.299, p-value = 0.017). **c.** In 13 dpf wild-type larvae, food intake correlates positively with body size (linear regression, R-squared: 0.3619, F: 6.805 on 1 and 12 DF, p-value: 0.02286), however in star:bPAC+, there is no significant correlation (R-squared: 0.1877, F: 2.773 on 1 and 12 DF, p-value: 0.1218). **d.** star:bPAC+ larvae are significantly smaller than wild types at 28 dpf and 120 dpf, but not at 5 dpf or 13 dpf (Two-way ANOVA with Tukey's test, *** p<0.001 for 28 and 120 dpf). **e**. Percentage of embryos that were fertilised by adult male star:bPAC+ fish is significantly lower compared to wild types (N=16,19 pairs, t = 2.7181, df = 31.072, p-value = 0.01064). **f.** Percentage of star:bPAC+ fish that survived to 2 months is significantly reduced, compared with wild types (Wilcoxon test, N=9, W = 65.5, p-value = 0.004315).

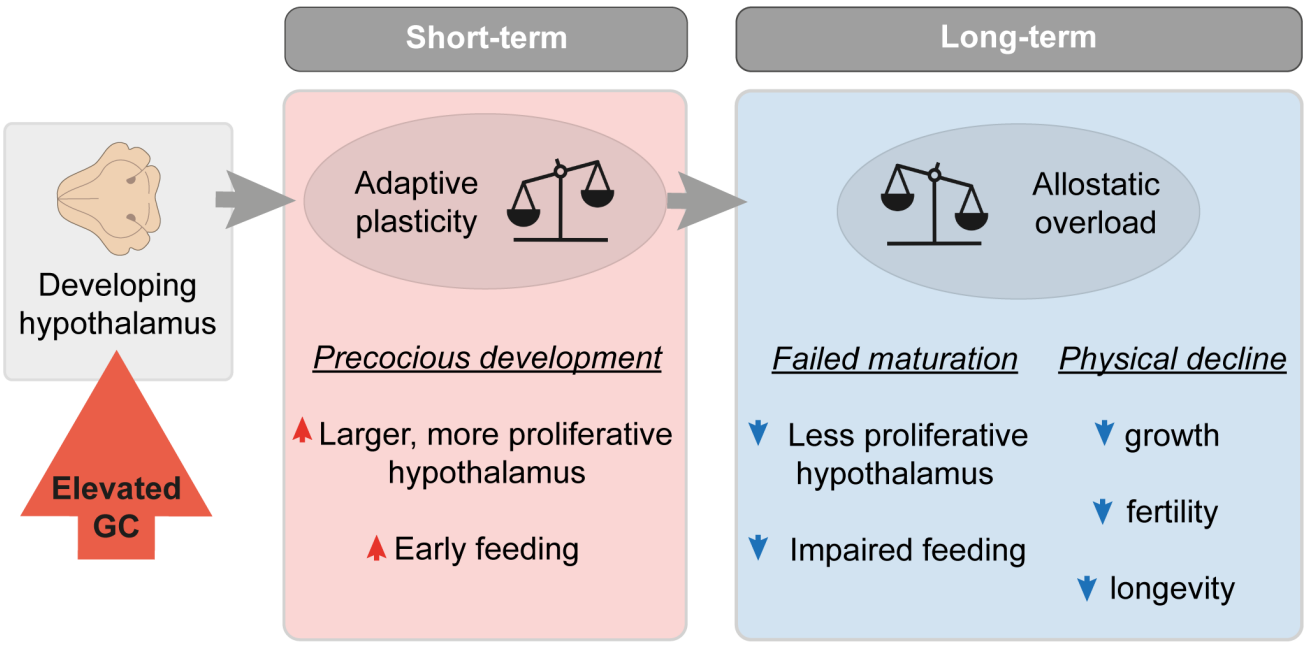

Figure 6. Model proposing how elevated GC alters the trajectory of hypothalamic development and function.

In our model of elevated GC, we suggest that in the short-term, GC exposure drives adaptive plasticity, whereby we observed precocious hypothalamic development. In the long-term, chronic GC exposure leads to an accumulation of allostatic load, leading to allostatic overload. We observed this via failed hypothalamic maturation during the larval stage, and subsequent early physical decline of exposed fish.

666 **Data Availability**

667 All sequenced reads for RNA-seq were deposited in European Nucleotide Archive (ENA,
668 PRJEB53713).

669

670 **Author contributions**

671 HE designed the study, performed the experiments, analysed the data, provided funding and wrote
672 the manuscript. MK designed, performed and analysed the RNA-seq experiments, and performed the
673 GR-ChIP. AT, JK, and MH performed some of the experiments. SR provided funding and contributed
674 to study design and manuscript writing.

675

676 **Conflict of interest**

677 SR holds a patent, European patent number 2928288 and US patent number 10,080,355: "A novel
678 inducible model of stress.". The remaining authors declare no known conflict of interest.

679

680 **Acknowledgements**

681 This project is supported by an award from The Dennis and Mireille Gillings Foundation to SR and
682 the German Federal Office for Education Research (grant number 01GQ1404) to SR. HE received
683 support from the Society for Endocrinology and Wellcome Trust Institutional Strategic Support Fund
684 3 scheme (ISSF3) to Translational Research Exchange @ Exeter. MH received support from the CN
685 Yang Scholars Programme at Nanyang Technological University. We would like to acknowledge the
686 support of Ms. Kathrin Domdera at the University of Mainz and the Exeter Aquatic Resources Centre
687 staff at the University of Exeter for expert zebrafish care as well as Dr Corin Liddle at Exeter
688 Bioimaging Centre for microscopy. We are grateful to Dr Elina Jacobs, Dr Kate Ellacott, Dr Steffen
689 Scholpp, and Professor Gil Levkowitz for feedback on the manuscript.

690

691 **References**

692 1. Chrousos GP. Stress and disorders of the stress system. *Nature Reviews Endocrinology* **5**,
693 374-381 (2009).
694

2. McKinlay CJD, Dalziel SR, Harding JE. Antenatal glucocorticoids: where are we after forty years? *J Dev Orig Health Dis* **6**, 127-142 (2015).

3. Wolford E*, et al.* Associations of antenatal glucocorticoid exposure with mental health in children. *Psychological Medicine* **50**, 247-257 (2020).

4. Ilg L, Klados M, Alexander N, Kirschbaum C, Li S-C. Long-term impacts of prenatal synthetic glucocorticoids exposure on functional brain correlates of cognitive monitoring in adolescence. *Scientific Reports* **8**, 7715 (2018).

5. Davis EP, Sandman CA, Buss C, Wing DA, Head K. Fetal glucocorticoid exposure is associated with preadolescent brain development. *Biol Psychiatry* **74**, 647-655 (2013).

6. Bale TL*, et al.* Early Life Programming and Neurodevelopmental Disorders. *Biol Psychiatry* **68**, 314-319 (2010).

7. Lupien SJ, McEwen BS, Gunnar MR, Heim C. Effects of stress throughout the lifespan on the brain, behaviour and cognition. *Nat Rev Neurosci* **10**, 434-445 (2009).

8. Danese A, McEwen BS. Adverse childhood experiences, allostasis, allostatic load, and age-related disease. *Physiol Behav* **106**, 29-39 (2012).

9. Moisiadis VG, Matthews SG. Glucocorticoids and fetal programming part 1: outcomes. *Nature Reviews Endocrinology* **10**, 391-402 (2014).

10. Suri D*, et al.* Early stress evokes age-dependent biphasic changes in hippocampal neurogenesis, BDNF expression, and cognition. *Biol Psychiatry* **73**, 658-666 (2013).

11. Mirescu C, Peters JD, Gould E. Early life experience alters response of adult neurogenesis to stress. *Nat Neurosci* **7**, 841-846 (2004).

12. Naninck EF*, et al.* Chronic early life stress alters developmental and adult neurogenesis and impairs cognitive function in mice. *Hippocampus* **25**, 309-328 (2015).

13. Lemaire V, Koehl M, Le Moal M, Abrous D. Prenatal stress produces learning deficits associated with an inhibition of neurogenesis in the hippocampus. *Proceedings of the National Academy of Sciences* **97**, 11032-11037 (2000).

14. Sawamoto A*, et al.* 3,5,6,7,8,3′,4′-Heptamethoxyflavone, a Citrus Flavonoid, Ameliorates Corticosterone-Induced Depression-like Behavior and Restores Brain-Derived Neurotrophic Factor Expression, Neurogenesis, and Neuroplasticity in the Hippocampus. *Molecules* **21**, 541 (2016).

15. Lehmann ML, Brachman RA, Martinowich K, Schloesser RJ, Herkenham M. Glucocorticoids Orchestrate Divergent Effects on Mood through Adult Neurogenesis. *The Journal of Neuroscience* **33**, 2961-2972 (2013).

16. Youssef M, Atsak P, Cardenas J, Kosmidis S, Leonardo ED, Dranovsky A. Early life stress delays hippocampal development and diminishes the adult stem cell pool in mice. *Sci Rep* **9**, 4120 (2019).

17. Bielefeld P*, et al.* Early life stress decreases cell proliferation and the number of putative adult neural stem cells in the adult hypothalamus. *Stress* **24**, 189-195 (2021).

749 18. Goodman T, Hajihosseini MK. Hypothalamic tanycytes-masters and servants of metabolic,
750 neuroendocrine, and neurogenic functions. *Front Neurosci* **9**, 387 (2015).
751
752 19. Choi M-K*, et al.* Developmental Glucocorticoid exposure in zebrafish primes expression of
753 genes linked to human psychiatric disorders. *bioRxiv*, 2023.2002.2013.528363 (2023).
754
755 20. Santulli G. *Adrenal Glands: From Pathophysiology to Clinical Evidence*. Nova Biomedical
756 (2015).
757
758 21. Eachus H*, et al.* Genetic Disruption of 21-Hydroxylase in Zebrafish Causes Interrenal
759 Hyperplasia. *Endocrinology* **158**, 4165-4173 (2017).
760
761 22. Oakes JA*, et al.* Ferredoxin 1b Deficiency Leads to Testis Disorganization, Impaired
762 Spermatogenesis, and Feminization in Zebrafish. *Endocrinology* **160**, 2401-2416 (2019).
763
764 23. Li N, Oakes JA, Storbeck K-H, Cunliffe VT, Krone NP. The P450 side-chain cleavage
765 enzyme Cyp11a2 facilitates steroidogenesis in zebrafish. *Journal of Endocrinology* **244**, 309-
766 321 (2020).
767
768 24. Oakes JA, Barnard L, Storbeck K-H, Cunliffe VT, Krone NP. 11β-Hydroxylase loss disrupts
769 steroidogenesis and reproductive function in zebrafish. *Journal of Endocrinology* **247**, 197-
770 212 (2020).
771
772 25. Shainer I*, et al.* Agouti-Related Protein 2 Is a New Player in the Teleost Stress Response
773 System. *Curr Biol* **29**, 2009-2019 e2007 (2019).
774
775 26. Wasserman-Bartov T, Admati I, Lebenthal-Loinger I, Sharabany J, Lerer-Goldshtein T,
776 Appelbaum L. Tsh Induces Agrp1 Neuron Proliferation in Oatp1c1-Deficient Zebrafish. *The*
777 *Journal of Neuroscience* **42**, 8214-8224 (2022).
778
779 27. Yokobori E*, et al.* Stimulatory effect of intracerebroventricular administration of orexin A on
780 food intake in the zebrafish, Danio rerio. *Peptides* **32**, 1357-1362 (2011).
781
782 28. Nagpal J, Eachus H, Lityagina O, Ryu S. Optogenetic induction of chronic glucocorticoid
783 exposure in early-life impairs stress-response in larval zebrafish. *bioRxiv*,
784 2022.2009.2009.507267 (2022).
785
786 29. Gutierrez-Triana JA*, et al.* Manipulation of Interrenal Cell Function in Developing Zebrafish
787 Using Genetically Targeted Ablation and an Optogenetic Tool. *Endocrinology* **156**, 3394-
788 3401 (2015).
789
790 30. Muthu V, Eachus H, Ellis P, Brown S, Placzek M. Rx3 and Shh direct anisotropic growth and
791 specification in the zebrafish tuberal/anterior hypothalamus. *Development (Cambridge,*
792 *England)* **143**, 2651-2663 (2016).
793
794 31. Pak T, Yoo S, Miranda-Angulo AL, Wang H, Blackshaw S. Rax-CreERT2 knock-in mice: a
795 tool for selective and conditional gene deletion in progenitor cells and radial glia of the retina
796 and hypothalamus. *PLoS One* **9**, e90381 (2014).
797
798 32. Kutsia M, Takeuchi Y, Ranawat N, Masai I. Single-cell transcriptome analysis reveals
799 heterogeneity and a dynamic regenerative response of quiescent radial glia in adult
800 zebrafish brain. *bioRxiv*, 2022.2007.2027.501663 (2022).
801
802 33. Ryu S*, et al.* Orthopedia homeodomain protein is essential for diencephalic dopaminergic
803 neuron development. *Curr Biol* **17**, 873-880 (2007).

34. Smith KL*, et al.* Overexpression of CART in the PVN Increases Food Intake and Weight Gain in Rats. *Obesity* **16**, 2239-2244 (2008).

35. Sundberg M, Savola S, Hienola A, Korhonen L, Lindholm D. Glucocorticoid hormones decrease proliferation of embryonic neural stem cells through ubiquitin-mediated degradation of cyclin D1. *J Neurosci* **26**, 5402-5410 (2006).

36. Bornstein SR*, et al.* Stress-inducible-stem cells: a new view on endocrine, metabolic and mental disease? *Molecular Psychiatry* **24**, 2-9 (2019).

37. Bornstein SR, Berger I, Steenblock C. Are Nestin-positive cells responsive to stress? *Stress* **23**, 662-666 (2020).

38. Ninomiya E, Hattori T, Toyoda M, Umezawa A, Hamazaki T, Shintaku H. Glucocorticoids promote neural progenitor cell proliferation derived from human induced pluripotent stem cells. *Springerplus* **3**, 527 (2014).

39. Heidt T*, et al.* Chronic variable stress activates hematopoietic stem cells. *Nat Med* **20**, 754-758 (2014).

40. Leung CS, Kosyk O, Welter EM, Dietrich N, Archer TK, Zannas AS. Chronic stress-driven glucocorticoid receptor activation programs key cell phenotypes and functional epigenomic patterns in human fibroblasts. *iScience* **25**, 104960 (2022).

41. Nürnberg E, Horschitz S, Schloss P, Meyer-Lindenberg A. Basal glucocorticoid receptor activation induces proliferation and inhibits neuronal differentiation of human induced pluripotent stem cell-derived neuronal precursor cells. *The Journal of Steroid Biochemistry and Molecular Biology* **182**, 119-126 (2018).

42. Yu S, He J. Stochastic cell-cycle entry and cell-state-dependent fate outputs of injury-reactivated tectal radial glia in zebrafish. *eLife* **8**, e48660 (2019).

43. Noorlander CW*, et al.* Antenatal glucocorticoid treatment affects hippocampal development in mice. *PLoS One* **9**, e85671 (2014).

44. Loi M, Koricka S, Lucassen PJ, Joels M. Age- and sex-dependent effects of early life stress on hippocampal neurogenesis. *Front Endocrinol (Lausanne)* **5**, 13 (2014).

45. Anacker C*, et al.* Glucocorticoid-related molecular signaling pathways regulating hippocampal neurogenesis. *Neuropsychopharmacology* **38**, 872-883 (2013).

46. Anacker C*, et al.* Antidepressants increase human hippocampal neurogenesis by activating the glucocorticoid receptor. *Molecular Psychiatry* **16**, 738-750 (2011).

47. Lee DA*, et al.* Tanycytes of the hypothalamic median eminence form a diet-responsive neurogenic niche. *Nat Neurosci* **15**, 700-702 (2012).

48. Coll AP, Farooqi IS, O'Rahilly S. The Hormonal Control of Food Intake. *Cell* **129**, 251-262 (2007).

49. Timper K, Brüning JC. Hypothalamic circuits regulating appetite and energy homeostasis: pathways to obesity. *Dis Model Mech* **10**, 679-689 (2017).

50. Zeltser LM. Feeding circuit development and early-life influences on future feeding behaviour. *Nat Rev Neurosci* **19**, 302-316 (2018).

51. Bolborea M, Pollatzek E, Benford H, Sotelo-Hitschfeld T, Dale N. Hypothalamic tanycytes generate acute hyperphagia through activation of the arcuate neuronal network. *Proc Natl Acad Sci U S A* **117**, 14473-14481 (2020).

52. Dantzer B*, et al.* Density Triggers Maternal Hormones That Increase Adaptive Offspring Growth in a Wild Mammal. *Science* **340**, 1215-1217 (2013).

53. Metcalfe NB, Monaghan P. Compensation for a bad start: grow now, pay later? *Trends in Ecology & Evolution* **16**, 254-260 (2001).

54. Lee W-S, Monaghan P, Metcalfe NB. Experimental demonstration of the growth rate–lifespan trade-off. *Proceedings of the Royal Society B: Biological Sciences* **280**, 20122370 (2013).

55. Lemaître J-F*, et al.* Early-late life trade-offs and the evolution of ageing in the wild. *Proceedings of the Royal Society B: Biological Sciences* **282**, 20150209 (2015).

56. McEwen BS, Wingfield JC. The concept of allostasis in biology and biomedicine. *Horm Behav* **43**, 2-15 (2003).

57. Monaghan P. Organismal stress, telomeres and life histories. *J Exp Biol* **217**, 57-66 (2014).

58. Jennings BJ, Ozanne SE, Hales CN. Nutrition, oxidative damage, telomere shortening, and cellular senescence: individual or connected agents of aging? *Mol Genet Metab* **71**, 32-42 (2000).

59. Costantini D, Marasco V, Møller AP. A meta-analysis of glucocorticoids as modulators of oxidative stress in vertebrates. *Journal of Comparative Physiology B* **181**, 447-456 (2011).

60. Pizzino G*, et al.* Oxidative Stress: Harms and Benefits for Human Health. *Oxid Med Cell Longev* **2017**, 8416763 (2017).

61. Barnes RP, Fouquerel E, Opresko PL. The impact of oxidative DNA damage and stress on telomere homeostasis. *Mech Ageing Dev* **177**, 37-45 (2019).

62. Burraco P, Díaz-Paniagua C, Gomez-Mestre I. Different effects of accelerated development and enhanced growth on oxidative stress and telomere shortening in amphibian larvae. *Scientific Reports* **7**, 7494 (2017).

63. Kumari R, Jat P. Mechanisms of Cellular Senescence: Cell Cycle Arrest and Senescence Associated Secretory Phenotype. *Frontiers in Cell and Developmental Biology* **9**, (2021).

64. Yang F*, et al.* Secretory galectin-3 induced by glucocorticoid stress triggers stemness exhaustion of hepatic progenitor cells. *J Biol Chem* **295**, 16852-16862 (2020).

65. Bose R, Moors M, Tofighi R, Cascante A, Hermanson O, Ceccatelli S. Glucocorticoids induce long-lasting effects in neural stem cells resulting in senescence-related alterations. *Cell Death Dis* **1**, e92 (2010).

66. Anchelin M, Alcaraz-Pérez F, Martínez CM, Bernabé-García M, Mulero V, Cayuela ML. Premature aging in telomerase-deficient zebrafish. *Dis Model Mech* **6**, 1101-1112 (2013).

67. Bobba-Alves N, *et al.* Chronic Glucocorticoid Stress Reveals Increased Energy Expenditure and Accelerated Aging as Cellular Features of Allostatic Load. *bioRxiv*, 2022.2002.2022.481548 (2022).

68. Bacila I, Cunliffe VT, Krone NP. Interrenal development and function in zebrafish. *Molecular and Cellular Endocrinology* **535**, 111372 (2021).

69. Eachus H, *et al.* Genetic Disruption of 21-Hydroxylase in Zebrafish Causes Interrenal Hyperplasia. *Endocrinology* **158**, 4165-4173 (2017).

70. Schouten M, *et al.* Circadian glucocorticoid oscillations preserve a population of adult hippocampal neural stem cells in the aging brain. *Molecular Psychiatry* **25**, 1382-1405 (2020).

71. Zannas AS, *et al.* Epigenetic upregulation of FKBP5 by aging and stress contributes to NF-κB–driven inflammation and cardiovascular risk. *Proceedings of the National Academy of Sciences* **116**, 11370-11379 (2019).

72. Prekovic S, *et al.* Glucocorticoid receptor triggers a reversible drug-tolerant dormancy state with acquired therapeutic vulnerabilities in lung cancer. *Nature Communications* **12**, 4360 (2021).

73. Westerfield M. *The zebrafish book. A guide for the laboratory use of zebrafish (Danio rerio)*, 4th Edition edn. University of Oregon Press (2000).

74. Choi M-K, Cook A, Eachus H, Tochwin A, Kuntz S, Ryu S. Comprehensive analysis methods for developmental GC exposed zebrafish. Preprint at http://dx.doi.org/10.17504/protocols.io.kxygx9ooog8j/v1 (2023).

75. Eachus H, Bright C, Cunliffe VT, Placzek M, Wood JD, Watt PJ. Disrupted-in-Schizophrenia-1 is essential for normal hypothalamic-pituitary-interrenal (HPI) axis function. *Hum Mol Genet* **26**, 1992-2005 (2017).

76. Herzog W, *et al.* Adenohypophysis formation in the zebrafish and its dependence on sonic hedgehog. *Dev Biol* **254**, 36-49 (2003).

77. Inoue D, Wittbrodt J. One for all--a highly efficient and versatile method for fluorescent immunostaining in fish embryos. *PLoS One* **6**, e19713 (2011).

78. Wolf A, Ryu S. Specification of posterior hypothalamic neurons requires coordinated activities of Fezf2, Otp, Sim1a and Foxb1.2. *Development* **140**, 1762-1773 (2013).

79. Randlett O, *et al.* Whole-brain activity mapping onto a zebrafish brain atlas. *Nat Methods* **12**, 1039-1046 (2015).

80. Idilli AI, *et al.* Expression of tert Prevents ALT in Zebrafish Brain Tumors. *Frontiers in Cell and Developmental Biology* **8**, (2020).

81. Eachus H, Choi MK, Ryu S. The Effects of Early Life Stress on the Brain and Behaviour: Insights From Zebrafish Models. *Front Cell Dev Biol* **9**, 657591 (2021).